Minimizing Training Signal Length for Power Amplifier Characterization and Linearization

Rahul Mushini, *Member, IEEE*, Yiyue Jiang, *Member, IEEE*, Miriam Leeser, *Life Senior Member, IEEE*, and John Dooley, *Member, IEEE*

***Abstract*— Wireless communication faces a significant challenge in meeting latency and power consumption requirements due, in large part, to the nonlinear behavior of power amplifiers (PAs) requiring digital predistortion (DPD). Calculating the parameters for DPD can be computationally demanding, especially with multiple transmitter paths in multiple-input–multiple-output (MIMO) systems. This research formulates a novel optimized training signal for DPD (OTS-DPD) that minimizes the number of samples needed to implement DPD while maintaining optimum PA linearization performance. Experimental validation of the DPD performance for the novel OTS-DPD signal demonstrates it outperforms a standard 5G orthogonal frequency division multiplexing (OFDM) signal and uses significantly fewer samples.**

***Index Terms*— Digital predistortion (DPD), hybrid beamforming, millimeter-wave (mmWave), multiple-input–multiple-output (MIMO), power amplifier (PA), power amplifier modeling, signal generation.**

I. Introduction

IN WIRELESS communication systems, the power amplifier (PA) is a significant cause of signal distortion in wireless transmitters. As a general observation, when operated at higher power, PAs exhibit nonlinear behavior and generate phase shifts that result in unwanted phase modulation. The PA output signal can also be distorted as a result of thermal effects or memory effects due to charge trapping [1].

Digital predistortion (DPD) can be employed to correct the distortion produced by PAs. Polynomial functions such as the generalized memory polynomial (GMP) [2] have been used successfully to perform DPD in the past. The computational burden with these polynomials increases with respect to the number of signal samples and severity of distortion.

Before implementing DPD, it is necessary to understand the nonlinear behavior of the PAs in terms of amplitude and phase distortion, and, to do this, a suitable training signal is needed. In [3], [4], and [5], two-tone signals can be used for PA characterization to a certain extent; however, two-tone signals are fundamentally limited in the extent they can probe the behavior of a PA. Efforts were made to design multitone characterization of training signals [6], [7], [8]. Multitones provide more frequency resolution than a single or two-tone measurement but require a large number of tones for capturing the nonlinearity. In [9], [10], and [11], PAs are characterized using a single or multiple pulse signal, which is a more precise technique than PA characterization using tones, but it is prone to the ringing effect [12]. Cappello et al. [12] used Gaussian pulses for PA characterization but it is not suitable for direct application in cellular networks as it does not comply with a wireless signal standard. Standards-compliant modulated signals can also be used for behavioral modeling and DPD. These approaches can typically require a large number of samples for training. Recent works have aimed to reduce the number of signal samples to reduce the computational workload [13], [14], [15], [16].

In this article, a novel optimized training signal for DPD (OTS-DPD) is presented that is created based on modern wireless signal standards. The samples are generated in such a way that the training signal excites the PA over its operating frequency, bandwidth, power levels, and power transitions. The proposed signal is optimized to minimize the number of training signal samples needed to model or predistort a PA.

II. Digital Predistortion

Many different DPD functions can be used to achieve a linear response from a nonlinear dynamic system, such as a PA. In this article, a GMP has been used as shown in [2] and the set of basis functions using GMP is represented as Y in this article. This basis function Y is of size $m \times n$, where m is the number of samples and n is the number of training signal samples used, which is determined by the order of nonlinearity, memory depth, and signal's leading and lagging envelope. As per [2], the inverse modeling is done by $\hat{x} = Y \times w$, where $\hat{x}$ is the estimated input using the output samples and w are the coefficients. Coefficients may be estimated using one of a variety of estimation algorithms. In this article, the QR decomposition estimation method is used. The QR decomposition estimator converts Y into

$$Y = Q \cdot R \tag{1}$$

where Q is $m \times n$ with orthonormal columns and R is an invertible $n \times n$ upper triangular matrix [17], [18]. The coefficients are determined by $w = R^{-1} Q^H x$, where x is the input signal [2].

Manuscript received 3 August 2023; accepted 13 September 2023. Date of publication 4 October 2023; date of current version 8 November 2023. This work was supported in part by the Science Foundation Ireland (SFI), MathWorks and in part by the European Regional Development Fund under Grant 18/CRT/6222. *(Corresponding author: Rahul Mushini.)*

Rahul Mushini and John Dooley are with the Department of Electronic Engineering, Maynooth University, Maynooth, W23 F2H6 Ireland (e-mail: rahul.mushini.2019@mumail.ie; john.dooley@mu.ie).

Yiyue Jiang and Miriam Leeser are with the Department of Electrical and Computer Engineering, Northeastern University, Boston, MA 02115 USA (e-mail: jiang.yiy@northeastern.edu; mel@coe.neu.edu).

Color versions of one or more figures in this letter are available at https://doi.org/10.1109/LMWT.2023.3317509.

Digital Object Identifier 10.1109/LMWT.2023.3317509

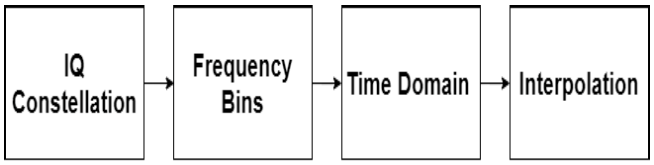

Fig. 1. Block diagram for signal construction.

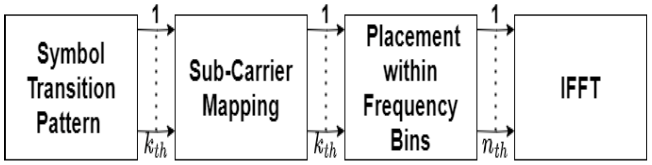

Fig. 2. (a) IQ constellation with vertical (↑) and horizontal (--→) transitions between symbols. (b) Placement of symbols within frequency bins.

Problem Statement: The computational burden of calculating the DPD coefficients from the above equation depends on two dimensions: n, which accounts for the number of DPD function coefficients, and m the number of signal samples for training. This manuscript presents a method to construct a complex envelope modulated signal that minimizes the number of samples m, needed to capture the nonlinear characteristics of the PA.

III. Optimized Training Signal Construction

Generating a orthogonal frequency division multiplexing (OFDM) signal follows the stages set out in Fig. 1. According to the specifications in [19], the radio frame comprises 307 200 samples within a 10-ms time interval, and the separation between each subcarrier is 15 kHz (Δf). This implies that 100 radio frames can be transmitted per second. Then, the sampling frequency f_s will be $f_s = 307\,200 \times (1000/10) = 30.72$ MSPS. Considering f_s and Δf, the number of frequency bins (N_{bin}) required is $N_{\text{bin}} = (f_s/\Delta f) = 2048$.

Now considering a signal with a bandwidth of 18 MHz with a subcarrier spacing of 15 kHz, the total number of occupied subcarriers can be determined using (BW/Δf) where BW is the bandwidth. Hence, the occupied frequency bin will be 1200 bins out of N_{bin} for an 18-MHz bandwidth signal. In this article, for generating approximately 100-MHz bandwidth signal, f_s was upsampled by a factor of 4 so that the new sampling frequency f_{snew} is 122.88 MSPS which means the new frequency bin N_{binnew} is 8192 bins. Hence, the number of subcarriers (f_{sub}) for ≈100-MHz bandwidth signal with Δf of 15 kHz should be 6600.

A. Calculate Ratio of Subcarriers to Use

Generating an OTS-DPD signal of a specified bandwidth can be achieved using a subset of the subcarriers. Selecting a sufficient but lower number of subcarriers will minimize the number of signal samples while maintaining the same format as the wireless transmission standard. The ratio of subcarriers needed to the total number of frequency bins will be

$$\text{Ratio} = \frac{N_{\text{binnew}}}{f_{\text{sub}}} \approx 1.24. \tag{2}$$

The frequency bin and the number of subcarriers can be scaled down as long as the ratio is maintained. Here, the frequency bin was scaled down by 64 which is equivalent to 128 frequency bins, and the number of subcarriers was, therefore, chosen to be 104. By utilizing (2), the new ratio comes to ≈1.23. Satisfying the ratio will ensure a 100-MHz bandwidth signal with an optimum number of samples. One point of note is that the subcarrier will occupy the center of the frequency bins except the dc or 0 Hz bin, that is, dc = ($N_{\text{bin}}/2$).

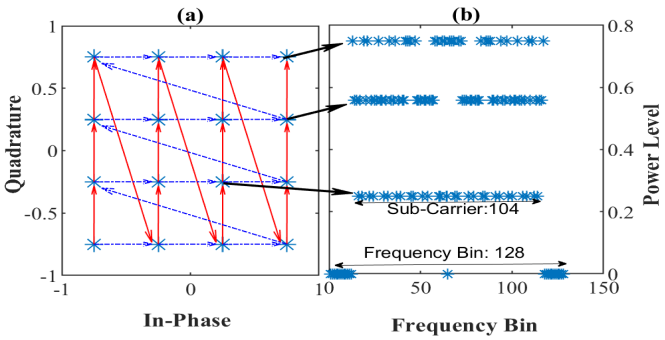

Fig. 3. Block diagram for symbol placement.

B. Selection of Subcarrier Subset

This section outlines the process of mapping symbols to select subcarriers to cover the PA's full range of operations in terms of the frequency and peak-to-average power ratio (PAPR). Two of the most important design objectives are that the signal must cover all the symbols and the PAPR should be similar to that of the RF system it will be applied to. The PAPR depends on the number of subcarriers mapped to the symbols. Therefore, the PAPR level can be managed by adding more or fewer symbols of specific power levels. The procedure is outlined in the following steps.

1) Symbols are selected on the constellation diagram of Fig. 2(a).
2) The next design choice is the transitions between the symbols. Any arbitrary transition between symbols can be chosen. In this work, the combination of horizontal and vertical symbol transitions was used as shown in Fig. 2(a).
3) The symbols are mapped to specific subcarriers as shown in Fig. 2(b), spanning the desired signal bandwidth.
4) Inverse fast Fourier transform (FFT) is used to convert the selection of frequency tones to a time-domain signal.

Finally, to minimize the number of time-domain samples for the signal, the number of symbol transitions will be set equal to the number of subcarriers, which, in this manuscript, is 104, including the dc component as mentioned in Section III-A. The symbols can be mapped to these subcarriers following any chosen strategy. In this work, we directly mapped the symbols following horizontal and vertical transitions as shown in Fig. 2(a). The transition between maximum and minimum absolute power levels was also included. The mapping onto the subcarriers in the frequency domain is shown in Fig. 2(b) and Fig. 3. This is then converted to the time domain using an inverse Fourier transform. This time-domain signal must be interpolated to match the system clock rate. The signal sample rate was changed to 983.04 MSPS from 122.88 MSPS to meet the RF transmitter system requirements, resulting in a signal length of 1024. Aside from managing the selection of symbols with different power levels, peak windowing crest factor

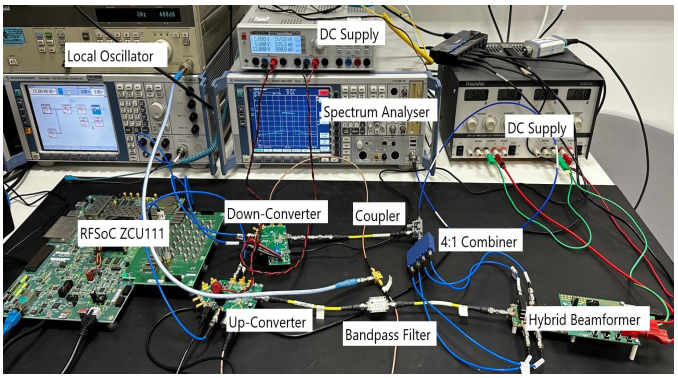

Fig. 4. Experimental test bench.

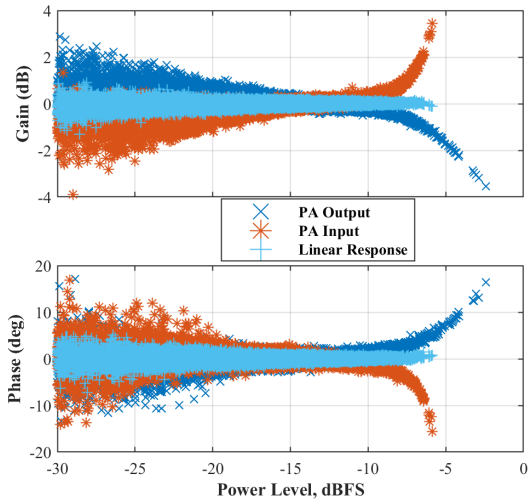

Fig. 5. Measured gain and phase offset versus input power.

reduction (CFR) [20] can be employed to adjust the PAPR and align it with the specified 10-dB PAPR requirement of 5G NR. In this article, two OTS-DPD signals are constructed using different symbol transitions and different combinations of power-level symbols and placement in allocated subcarriers. This will allow the developed DPD actuator to adapt to the nonlinearity generated for different frequencies, power levels, and power transitions. One should note that both OTS-DPD signals used in this manuscript were tailored to have the same PAPR level.

IV. Experimental Results

The proposed training was experimentally validated using a test bench shown in Fig. 4. The RFSOC ZCU111 was utilized for transmitting and receiving the signal. The signal was upconverted and filtered to ≈28 GHz, fed to the PAs in the beamformer module, and the output was sensed using a 30-dB coupled output port. The downconverted signal was processed in MATLAB. As a first test, PA characterization was carried out using a large 81 920 sample 5G NR signal to model the PA. The parameter used for validating the accuracy of the PA model was error vector magnitude (EVM) which was −47.5 dB. To achieve comparable accuracy for a PA model calculated using the proposed optimized training signal, only 1024 samples were required.

For testing, a 5G NR signal was passed through the DPD actuator developed using the OTS-DPD signal for predistorting

TABLE I
EVM and ACPR Performance Comparison

Signal	# of Samples	EVM (dB)	ACPR (dBc)
Before DPD	81920	-28.37	-33.68
5G NR PK	1024	-30.23	-36.14
5G NR PK	8192	-43.34	-45.80
5G NR PK	81920	-47.42	-47.82
5G NR PDF	4096	-43.47	-43.98
OTS-DPD Signal	1024	-45.05	-47.70

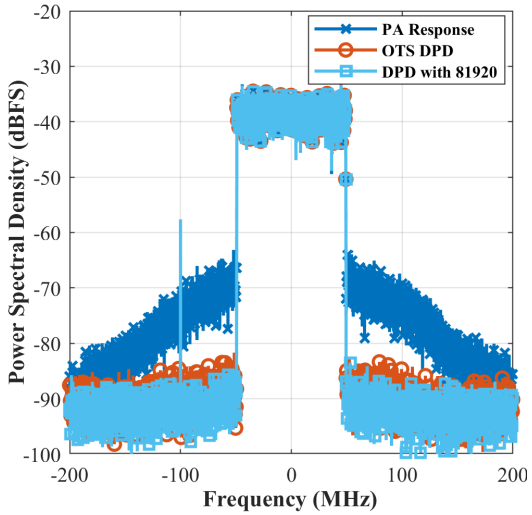

Fig. 6. Frequency response plot using measured result.

the signal which in turn was fed to the PA. This leads to successful linearization for the PA with compression of ≈4 dB as can be seen from Fig. 5. Table I compares signal-processing methods for PA linearization, focusing on the benefits of using the OTS-DPD signal. The proposed method was compared against two methods for developing the DPD actuator: one is based on selecting the signal samples around the peak power samples (5G NR PK), and the other by maintaining the probability density function of the signal (5G NR pdf) as shown in [16]. With only 1024 samples, the OTS-DPD signal demonstrates significant improvements in EVM and adjacent channel power ratio (ACPR). EVM is reduced from −28.37 to −45.05 dB, while ACPR improves from −33.68 to −47.70 dBc which is evident in Fig. 6. These results underscore the effectiveness of the OTS-DPD signal in minimizing sample requirements while maintaining optimal linearization performance. For wireless communication systems aiming for enhanced efficiency and signal quality, the OTS-DPD signal presents a compelling choice.

V. Conclusion

In this article, the authors introduce a novel method of constructing an optimized training signal for PA behavioral modeling and/or DPD, using modern wireless signal standards. By using this OTS-DPD signal, the nonlinear information from the PA can be captured with a fraction of the training samples compared to other state-of-the-art solutions. The effectiveness of the proposed training signal was experimentally validated for an mmWave frequency hardware testbench, comparing the DPD actuators obtained with the OTS-DPD signal to that obtained using a standard 5G NR signal.

REFERENCES

[1] F. H. Raab et al., "RF and microwave power amplifier and transmitter technologies—Part 1," *High Freq. Electron.*, vol. 2, no. 3, pp. 22–36, 2003.

[2] D. R. Morgan, Z. Ma, J. Kim, M. G. Zierdt, and J. Pastalan, "A generalized memory polynomial model for digital predistortion of RF power amplifiers," *IEEE Trans. Signal Process.*, vol. 54, no. 10, pp. 3852–3860, Oct. 2006.

[3] C. J. Clark, C. P. Silva, A. A. Moulthrop, and M. S. Muha, "Power-amplifier characterization using a two-tone measurement technique," *IEEE Trans. Microw. Theory Techn.*, vol. 50, no. 6, pp. 1590–1602, Jun. 2002.

[4] Y. Yang, J. Yi, J. Nam, and B. Kim, "Behavioral modeling of high power amplifiers based on measured two-tone transfer characteristics," *Channels*, vol. 4, p. 5G, Dec. 2000.

[5] T. R. Cunha, F. M. Barradas, and J. C. Pedro, "The two-tone model for power amplifier modeling," in *Proc. 46th Eur. Microw. Conf. (EuMC)*, Oct. 2016, pp. 1087–1090.

[6] N. B. De Carvalho and J. C. Pedro, "Multitone frequency-domain simulation of nonlinear circuits in large- and small-signal regimes," *IEEE Trans. Microw. Theory Techn.*, vol. 46, no. 12, pp. 2016–2024, Dec. 1998.

[7] F. L. Ogboi et al., "High bandwidth investigations of a baseband linearization approach formulated in the envelope domain under modulated stimulus," in *Proc. 44th Eur. Microw. Conf.*, Oct. 2014, pp. 1305–1308.

[8] T. Cappello, A. Duh, T. W. Barton, and Z. Popovic, "A dual-band dual-output power amplifier for carrier aggregation," *IEEE Trans. Microw. Theory Techn.*, vol. 67, no. 7, pp. 3134–3146, Jul. 2019.

[9] A. Santarelli et al., "A double-pulse technique for the dynamic I/V characterization of GaN FETs," *IEEE Microw. Wireless Compon. Lett.*, vol. 24, no. 2, pp. 132–134, Feb. 2014.

[10] S. Bensmida et al., "Power amplifier memory-less pre-distortion for 3GPP LTE application," in *Proc. Eur. Microw. Conf. (EuMC)*, Sep. 2009, pp. 1433–1436.

[11] G. P. Gibiino, F. F. Tafuri, T. S. Nielsen, D. Schreurs, and A. Santarelli, "Pulsed NVNA measurements for dynamic characterization of RF PAs," in *Proc. IEEE Int. Microw. RF Conf. (IMaRC)*, Dec. 2014, pp. 92–95.

[12] T. Cappello, Z. Popovic, K. Morris, and A. Cappello, "Gaussian pulse characterization of RF power amplifiers," *IEEE Microw. Wireless Compon. Lett.*, vol. 31, no. 4, pp. 417–420, Apr. 2021.

[13] Z. Wang, J. Dooley, K. Finnerty, and R. Farrell, "Selection of compressed training data for RF power amplifier behavioral modeling," in *Proc. 10th Eur. Microw. Integr. Circuits Conf. (EuMIC)*, Sep. 2015, pp. 53–56.

[14] R. Zhu, "Gradient-based sampling: An adaptive importance sampling for least-squares," in *Proc. Adv. Neural Inf. Process. Syst.*, vol. 29, 2016. [Online]. Available: https://papers.nips.cc/paper_files/paper/2016

[15] J. Kral, T. Gotthans, R. Marsalek, M. Harvanek, and M. Rupp, "On feedback sample selection methods allowing lightweight digital predistorter adaptation," *IEEE Trans. Circuits Syst. I, Reg. Papers*, vol. 67, no. 6, pp. 1976–1988, Jun. 2020.

[16] Z. Han, Y. Jiang, R. Mushini, J. Dooley, and M. Leeser, "Hardware software codesign of applications on the Edge: Accelerating digital Pre-Distortion for wireless communications," in *Proc. IEEE High Perform. Extreme Comput. Conf. (HPEC)*, Sep. 2022, pp. 1–6.

[17] J. Jake, E. Mwangi, and K. Langat, "Spectral re-growth suppression in the FBMC-OQAM signal under the non-linear behavior of a power amplifier," *Eng., Technol. Appl. Sci. Res.*, vol. 9, no. 5, pp. 4801–4807, Oct. 2019.

[18] W. Gao and W. Gao, "Linearization techniques for RF power amplifiers," in *Energy and Bandwidth-Efficient Wireless Transmission*. Springer, 2017, pp. 253–289. [Online]. Available: https://link.springer.com/chapter/10.1007/978-3-319-44222-8_5

[19] ETSI. (2022). *ETSI-TS-136-211-v12.9.0-LTE*. [Online]. Available: https://www.etsi.org/deliver/etsi_ts/138100_138199/13814102/17.05.00_60/ts_13814102v170500p.pdf

[20] O. Vaananen, J. Vankka, and K. Halonen, "Simple algorithm for peak windowing and its application in GSM, EDGE and WCDMA systems," *IEE Proc. Commun.*, vol. 152, no. 3, pp. 357–362, Jun. 2005.